Unraveling the essential role of CysK in CDI toxin activation

Parker M. Johnson[a,1], Christina M. Beck[b,1], Robert P. Morse[a], Fernando Garza-Sánchez[b], David A. Low[b,c], Christopher S. Hayes[b,c,2], and Celia W. Goulding[a,d,2]

[a]Department of Molecular Biology and Biochemistry, University of California, Irvine, CA 92697; [b]Department of Molecular, Cellular and Developmental Biology, University of California, Santa Barbara, CA 93106-9625; [c]Biomolecular Science and Engineering Program, University of California, Santa Barbara, CA 93106-9625; and [d]Department of Pharmaceutical Sciences, University of California, Irvine, CA 92697

Edited by Bonnie L. Bassler, Princeton University and Howard Hughes Medical Institute, Princeton, NJ, and approved July 13, 2016 (received for review May 4, 2016)

Contact-dependent growth inhibition (CDI) is a widespread mechanism of bacterial competition. CDI$^+$ bacteria deliver the toxic C-terminal region of contact-dependent inhibition A proteins (CdiA-CT) into neighboring target bacteria and produce CDI immunity proteins (CdiI) to protect against self-inhibition. The CdiA-CT^{EC536} deployed by uropathogenic *Escherichia coli* 536 (EC536) is a bacterial toxin 28 (Ntox28) domain that only exhibits ribonuclease activity when bound to the cysteine biosynthetic enzyme *O*-acetylserine sulfhydrylase A (CysK). Here, we present crystal structures of the CysK/CdiA-CT^{EC536} binary complex and the neutralized ternary complex of CysK/CdiA-CT/CdiI^{EC536}. CdiA-CT^{EC536} inserts its C-terminal Gly-Tyr-Gly-Ile peptide tail into the active-site cleft of CysK to anchor the interaction. Remarkably, *E. coli* serine *O*-acetyltransferase uses a similar Gly-Asp-Gly-Ile motif to form the "cysteine synthase" complex with CysK. The cysteine synthase complex is found throughout bacteria, protozoa, and plants, indicating that CdiA-CT^{EC536} exploits a highly conserved protein–protein interaction to promote its toxicity. CysK significantly increases CdiA-CT^{EC536} thermostability and is required for toxin interaction with tRNA substrates. These observations suggest that CysK stabilizes the toxin fold, thereby organizing the nuclease active site for substrate recognition and catalysis. By contrast, Ntox28 domains from Gram-positive bacteria lack C-terminal Gly-Tyr-Gly-Ile motifs, suggesting that they do not interact with CysK. We show that the Ntox28 domain from *Ruminococcus lactaris* is significantly more thermostable than CdiA-CT^{EC536}, and its intrinsic tRNA-binding properties support CysK-independent nuclease activity. The striking differences between related Ntox28 domains suggest that CDI toxins may be under evolutionary pressure to maintain low global stability.

bacterial competition | structural biology | toxin chaperone | tRNase activity

Bacteria have evolved diverse mechanisms to communicate and compete with neighboring microorganisms. One such mechanism is contact-dependent growth inhibition (CDI), which mediates the transfer of protein toxins between Gram-negative bacterial cells. CDI systems are distributed throughout α-, β-, and γ-proteobacteria and are particularly common in pathogens (1). CDI is mediated by the CdiB/CdiA family of two-partner secretion proteins. CdiB is an Omp85-family transporter that exports and assembles CdiA effectors onto the cell surface. CdiA proteins share homology with filamentous hemagglutinin adhesins and are thought to form long filaments projecting from the inhibitor cell. CdiA recognizes specific receptors on susceptible bacteria and delivers its toxic C-terminal domain (CdiA-CT) to inhibit target-cell growth (2). CDI$^+$ bacteria also produce CdiI immunity proteins, which bind CdiA-CT domains and neutralize their toxic activity to protect against self-inhibition. The CdiA-CT region is highly polymorphic between bacteria, with sequences diverging abruptly after the Val-Glu-Asn-Asn (VENN) peptide motif within the conserved pretoxin domain (Pfam: PF04829) (3, 4). CdiA-CT diversity reflects the variety of toxins deployed during CDI, with most experimentally characterized toxins exhibiting distinct nuclease activities (3, 5–7). CdiI immunity proteins are also variable and only neutralize their cognate CdiA-CT toxins. Thus, CDI is thought to mediate interstrain competition, with toxin/immunity protein variability providing a mechanism to discriminate between self and non-self (1, 2).

Previous studies on the CDI toxin from uropathogenic *Escherichia coli* 536 (EC536) revealed that it possesses latent anticodon nuclease activity against all tRNA isoacceptors (8). The CdiA-CT^{EC536} region is composed of two domains that have distinct functions during CDI (9). The extreme C-terminal domain is an Ntox28 RNase family member (Pfam: PF15605) and is responsible for growth-inhibition activity (3, 8). The N-terminal domain facilitates translocation of the tethered nuclease into the cytosol of target bacteria (9). Although CdiA-CT^{EC536} rapidly cleaves tRNA in vivo, the purified toxin has no detectable nuclease activity in vitro (8). Using biochemical approaches, we discovered that CdiA-CT^{EC536} is activated when bound to the biosynthetic enzyme *O*-acetylserine sulfhydrylase-A (CysK). CysK is one of two isoenzymes (along with CysM) that catalyze the final reaction in cysteine synthesis. In bacteria and plants, CysK is found in the "cysteine synthase" complex together with CysE—the serine *O*-acetyltransferase responsible for the penultimate step of cysteine synthesis (10). Formation of the cysteine synthase complex requires the C-terminal tail of CysE, which inserts into the CysK active site (11). The C-terminal Ile

Significance

Contact-dependent growth inhibition (CDI) systems produce toxins that inhibit competing bacteria and immunity proteins that protect against self-inhibition. The CDI toxin deployed by *Escherichia coli* 536 is a nuclease that only cleaves transfer RNA (tRNA) molecules when bound to the biosynthetic enzyme *O*-acetylserine sulfhydrylase (CysK). Here, we present crystal structures of the activated CysK/toxin binary complex and the neutralized CysK/toxin/immunity protein ternary complex. CysK significantly increases toxin thermostability and promotes its interaction with tRNA substrates. Collectively, our results indicate that CysK stabilizes the toxin fold, thereby organizing the nuclease active site for substrate recognition and catalysis. We propose that the *E. coli* 536 toxin may need to unfold when transferred between bacteria and that its interaction with CysK could ensure reactivation after entry into target cells.

Author contributions: P.M.J., C.M.B., R.P.M., F.G.-S., D.A.L., C.S.H., and C.W.G. designed research; P.M.J., C.M.B., R.P.M., and F.G.-S. performed research; P.M.J., C.M.B., R.P.M., F.G.-S., C.S.H., and C.W.G. analyzed data; and C.S.H. and C.W.G. wrote the paper.

The authors declare no conflict of interest.

This article is a PNAS Direct Submission.

Data deposition: The atomic coordinates and structure factors have been deposited in the Protein Data Bank, www.pdb.org (PDB ID codes 5J5V and 5J43).

[1]P.M.J. and C.M.B. contributed equally to this work.

[2]To whom correspondence may be addressed. Email: celia.goulding@uci.edu or christopher.hayes@lifesci.ucsb.edu.

This article contains supporting information online at www.pnas.org/lookup/suppl/doi:10.1073/pnas.1607112113/-/DCSupplemental.

residue of CysE is particularly critical and interacts with the CysK active site using the same contacts as the enzyme substrate *O*-acetylserine (12, 13). Although CysK and CysM share 58% sequence identity, CysE does not interact stably with the CysM isoenzyme (14). The CdiA-CT^{EC536} toxin carries a C-terminal Gly-Tyr-Gly-Ile (GYGI) peptide motif that appears to mimic the Gly-Asp-Gly-Ile (GDGI) tail of *E. coli* CysE. Moreover, *O*-acetylserine blocks the binding of both CysE and CdiA-CT^{EC536} to CysK (8, 10), indicating that CdiA-CT^{EC536} also inserts its C-terminal tail into the CysK active-site cleft. Remarkably, other proteins mimic CysE to bind CysK (15). In *Bacillus* species, the CymR transcription factor uses its C-terminal Met-Phe-Tyr-Ile tail to bind CysK, and modulation of this interaction controls the *cys* regulon (16). Perhaps more intriguing is EGL-9, an O_2-sensing prolyl hydroxylase from *Caenorhabditis elegans* that binds a CysK homolog (CYSL-1) using a C-terminal Ile residue (17). The resulting complex senses O_2 tension indirectly through hydrogen sulfide, which accumulates during hypoxia. Sulfide binds the CYSL-1 active site and displaces the C terminus of EGL-9. Once liberated, EGL-9 hydroxylates HIF-1 to initiate transcriptional responses to hypoxia (17). Thus, CysK and its homologs have been coopted to regulate gene expression in bacteria and eukaryotes.

To gain mechanistic insight into toxin activation, we solved crystal structures of the CdiA-CT^{EC536} toxin in binary complex with CysK, and in ternary complex with CysK and CdiI^{EC536} immunity protein. The nuclease domain forms a small four-helix bundle with no structural similarity to other known RNase families. Two toxins bind to each CysK homodimer, and the C-terminal GYGI peptide of the nuclease inserts into the CysK active-site cleft as predicted by previous studies (8). Structure-guided mutagenesis revealed a putative catalytic triad of Asp155, His178, and Glu181 in the nuclease domain. The predicted nuclease active site is occluded by immunity protein in the CysK/CdiA-CT/CdiI^{EC536} structure, suggesting that CdiI^{EC536} blocks the binding of tRNA substrates to the toxin. Intriguingly, Ntox28 homologs from Gram-positive bacteria lack the C-terminal GYGI motif, suggesting that they do not require CysK-mediated activation. We tested this prediction using Tox28^{Rlac} from *Ruminococcus lactaris* and confirmed that the domain possesses CysK-independent tRNase activity. Moreover, Tox28^{Rlac} is significantly more stable to thermal denaturation than CdiA-CT^{EC536} and possesses intrinsic tRNA-binding activity. By contrast, CysK is required for tRNA binding to CdiA-CT^{EC536}. Collectively, these findings suggest that CysK is recruited to stabilize CdiA-CT^{EC536}, thereby organizing the active site to promote substrate binding and catalysis.

Results

We generated a binary complex of CysK bound to inactive CdiA-CT^{EC536} toxin that contains the His178Ala mutation (numbered from Val1 of the VENN motif). The CysK/CdiA-CT(H178A)^{EC536} complex crystallized in space group $P4_1$, and the structure was solved to 2.7 Å resolution (Table S1). Like other *O*-acetylserine sulfhydrylases (18), *E. coli* CysK is homodimeric and contains a pyridoxal 5′-phosphate (PLP) cofactor in Schiff-base linkage to Lys42. CysK in the binary complex has an "open" active-site conformation, similar to the structure of unliganded CysK from *Salmonella* Typhimurium (rmsd of 0.5 Å over all 312 α-carbons) (18). Thus, the toxin does not induce the "closed" conformation observed when CysK contains substrate covalently bound to PLP in the active site (19). As we have found in other CdiA-CT toxin structures (5, 6, 20), only the C-terminal nuclease domain (residues Lys127–Ile227) is resolved in the final model. The CdiA-CT^{EC536} nuclease domain consists of four α-helices. Three long helices (α1, α3, and α4) form a bundle capped by the shorter helix α2 (Fig. 1*A*). Helices α2 and α3 are connected by the long flexible loop L2, which was modeled predominately as Ala residues. Two CdiA-CT^{EC536} nuclease domains bind to the CysK dimer, but the toxins make no contact with one another (Fig. 1*A*), suggesting that they bind independently. The C-terminal tail of the nuclease domain

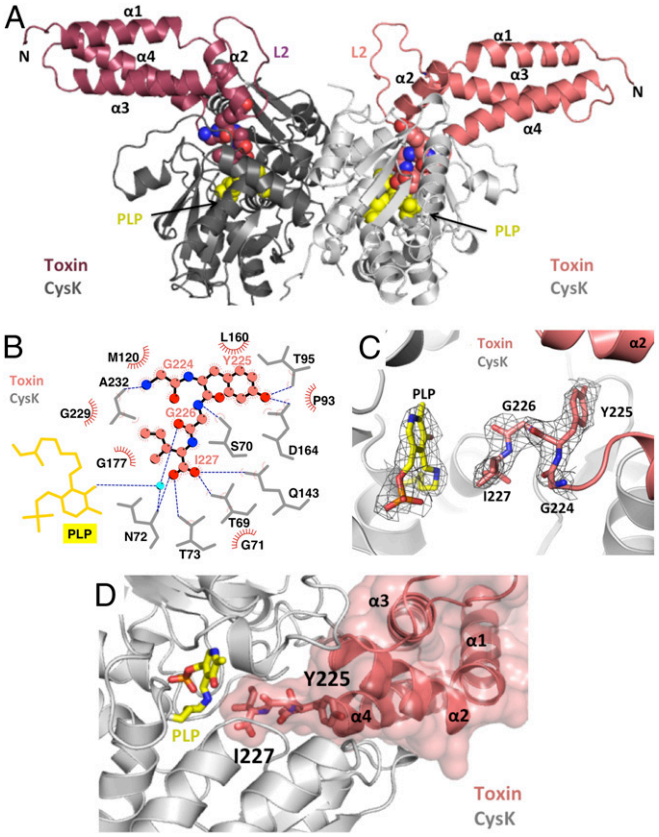

Fig. 1. The CysK/CdiA-CT^{EC536} binary complex. (*A*) Crystal structure of the CysK/CdiA-CT^{EC536} complex. Secondary structure elements of the toxin nuclease domain are indicated together with flexible loop L2. The C-terminal GYGI peptides of CdiA-CT^{EC536} and CysK-bound pyridoxyl 5′-phosphate (PLP) are rendered as spheres. (*B*) GYGI peptide interaction network. CdiA-CT^{EC536} residues Gly224, Tyr225, Gly226, and Ile227 are shown in spheres, and CysK residues and PLP are rendered as gray and yellow sticks, respectively. A water molecule is shown as a cyan sphere. Red arcs represent hydrophobic interactions, and blue dashed lines indicate H-bonds. The interaction network was produced using LigPlot. (*C*) Interaction between CdiA-CT^{EC536} C-terminal GYGI peptide and the CysK active site. The CdiA-CT^{EC536} GYGI peptide and CysK PLP are shown in stick representation. The $2F_o - F_c$ electron density map of the CdiA-CT^{EC536} GYGI peptide and CysK PLP is shown in gray mesh and contoured at 1.0 σ. (*D*) The CdiA-CT^{EC536} toxin domain exploits shape complementarity to bind the CysK active-site cleft. Residues Gly224–Ile227 and PLP are shown in stick representation.

inserts into the CysK active site, with the GYGI peptide backbone forming a network of hydrogen bonds (H-bonds) with CysK (Fig. 1*B* and Table S2). The toxin's C-terminal Ile227 residue is positioned in close proximity to the active-site PLP and forms H-bonds with Thr69, Asn72, Thr73, and Gln143 of CysK (Fig. 1 *B* and *C*). These latter contacts have been observed in structures of CysE C-terminal peptides bound to the CysK active site (13, 21, 22). The side-chain of Tyr225 H-bonds to CysK residues Thr95 and Asp164 (Fig. 1*B* and Table S2). The GYGI tail interactions are buttressed by additional H-bonds and salt bridges emanating from toxin helices α2, α3, and α4 (Table S2). Residues within α2 (Leu160, Ile156, Ile157, and Met163), α3 (Met179 and Leu186), and α4 (Leu222) also form hydrophobic interactions with CysK, and the toxin helical bundle exploits shape complementarity to fit into the CysK active-site cleft (Fig. 1*D*). Overall, the complex interface is 1,280 Å^2, burying 9.2% and 19.4% of the solvent-accessible surface areas of CysK and CdiA-CT^{EC536}, respectively.

E. coli CysK and CysM share related structures (rmsd of 1.8 Å over 285/292 α-carbons) but differ significantly in the loop L17 region at the entrance of the active-site cleft (Fig. 2*A*). CysK

BIOCHEMISTRY

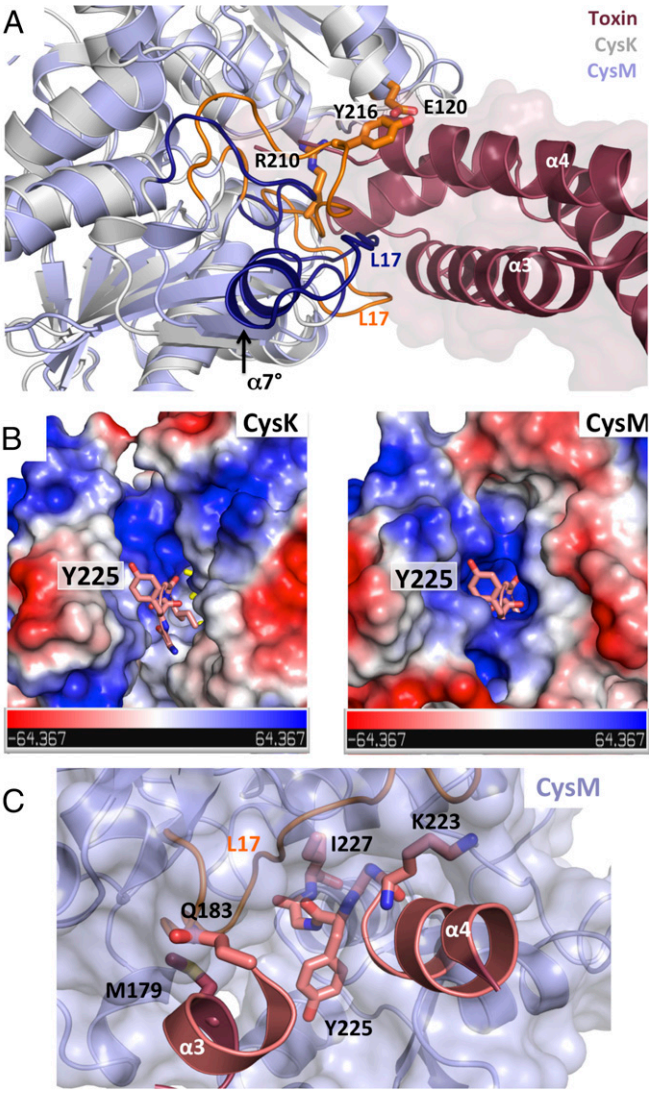

Fig. 2. Comparison of *E. coli* CysK and CysM structures. (*A*) Superimposition of *E. coli* CysM (PDB ID code 2BHT) onto the CysK/CdiA-CT^{EC536} binary complex. The divergent loop L17 regions are highlighted in orange for CysM and dark blue for CysK. The additional helix α7° in CysK is indicated, as are CysM residues that clash with the surface of the nuclease domain. (*B*) Electrostatic surface representations of CysK and CysM. Electric isopotentials of +64.4 kT/e and –64.4 kT/e are shown in blue and red, respectively. The C-terminal GYGI peptide of CdiA-CT^{EC536} is shown in stick representation. (*C*) CdiA-CT^{EC536} modeled onto the CysM structure. Toxin residues that clash with loop L17 of CysM are shown in stick representation.

contains 16 extra residues in loop L17 that introduce an additional α-helix (α7°) (Fig. 2*A* and Fig. S1). The differences in loop L17 have profound effects on the landscape and electrostatic surface potential of each active-site cleft (Fig. 2*B*) (12, 23). Superimposition of CdiA-CT^{EC536} onto the CysM structure produces several clashes with the C-terminal GYGI peptide (Fig. 2*B*). Moreover, the CysM active site contains no hydrophobic pockets capable of accommodating the side-chains of toxin residues Ile227 and Tyr225. Residues Lys223 and Gly224 at the end of toxin helix α4 and Met179 and Gln183 within helix α3 each clash with the surface of CysM loop L17 (Fig. 2*C*). Thus, CdiA-CT^{EC536} and CysE both exploit differences in loop L17 sequence and structure to bind CysK specifically.

The CdiI^{EC536} immunity protein binds to CysK/CdiA-CT^{EC536}, forming a neutralized ternary complex (8). The crystal structure of this ternary complex shows that immunity protein binds to each toxin to form a dimer of heterotrimers (Fig. 3*A*). The CysK and CdiA-CT^{EC536} structures and interactions are very similar in the binary and ternary complexes (rmsd of 0.25 Å over all α-carbons; Table S3), indicating that the immunity protein does not grossly alter toxin conformation. CdiI^{EC536} is a single domain composed of one 3_{10}- and eight α-helices arranged in four stacked layers to form an antiparallel spiral (Fig. 3*B*). A DALI server (24) search indicates that CdiI^{EC536} does not share structural homology with other known antitoxins or immunity proteins (Table S4). The immunity protein interacts exclusively with the nuclease domain of CdiA-CT^{EC536} and makes no contacts with CysK (Fig. 3*A*). Flexible loop L2 of the nuclease domain interacts extensively with CdiI^{EC536}, stabilizing the loop and allowing its side-chains to be fully resolved in the ternary complex (Fig. 3*C*). Fifteen H-bonds and ion pairs connect CdiA-CT^{EC536} helix α3 to helices α2*, α4*, and α6* of CdiI^{EC536} (Fig. 2*C* and Table S5). Additionally, toxin residue Trp176 from loop L2 fits into a hydrophobic pocket formed by Ile8, Ile11, Leu23, Trp26, Phe27, and Leu51 of CdiI^{EC536} (Fig. 3*D*). The toxin/immunity protein interface is 1,034 Å^2, burying 16.6% and 12.7% of the solvent-accessible surface areas of CdiA-CT^{EC536} and CdiI^{EC536}, respectively. Comparisons of different Ntox28 domains and their predicted immunity proteins reveal that many of the interacting residues are conserved throughout the toxin/immunity family (Fig. S2).

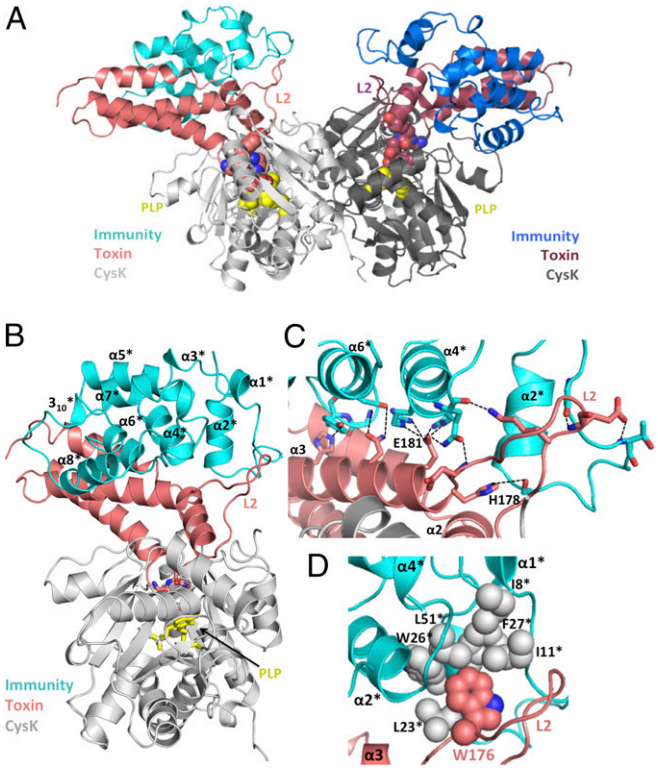

Fig. 3. The CysK/CdiA-CT/CdiI^{EC536} ternary complex. (*A*) Crystal structure of the CysK/CdiA-CT/CdiI^{EC536} complex. The C-terminal GYGI peptide of CdiA-CT^{EC536} and CysK-bound pyridoxyl 5′-phosphate (PLP) are rendered as spheres. The ternary complex is presented in the same orientation as Fig. 1*A*. (*B*) Monomeric version of the ternary complex. CdiI^{EC536} secondary structure elements are outlined and indicated with superscripted asterisks (*). The C-terminal GYGI peptide of the toxin and PLP are shown as sticks. (*C*) H-bonding network between CdiA-CT^{EC536} and CdiI^{EC536}. Interacting residues are shown in stick representation, and dashed lines indicate H-bonds. Active-site residues His178 and Glu181 from L2 and α3 of CdiA-CT^{EC536} interact with α2*, α4*, and α6* of CdiI^{EC536}. (*D*) Hydrophobic interactions between CdiA-CT^{EC536} and CdiI^{EC536}. CdiA-CT^{EC536} Trp176 binds into a hydrophobic pocket formed by CdiI^{EC536}.

A DALI search indicates that the CdiA-CT^{EC536} nuclease domain does not share structural homology with other known RNases (Table S4). The domain also lacks an obvious tRNA-binding pocket, but previous work suggests that His178 is an active-site residue (Fig. 4*A* and Fig. S2*A*) (8). Therefore, we used site-directed mutagenesis to probe residues in the vicinity of His178 for roles in growth inhibition. CdiA-CT^{EC536} expression plasmids were introduced into *E. coli cysK*$^+$ and Δ*cysK* strains, and transformants were selected on media supplemented with either glucose to suppress, or arabinose to induce, toxin expression. The WT construct was lethal when introduced into *cysK*$^+$ cells under any condition but had no effect on Δ*cysK* cell growth even when induced with arabinose (Fig. 4*B*). This result illustrates *cysK*-dependent toxicity for comparison with mutated CdiA-CT^{EC536} variants. CdiA-CT^{EC536} residues Asp155 and Glu181 cluster near His178 (Fig. 4*A*) and are completely conserved in known Ntox28 domains (Fig. S2*A*), suggesting functional importance. Asp155Ala and Glu181Ala mutations abolished growth inhibition activity, showing the same phenotype as the His178Ala mutation (Fig. 4*B*). Thr185 is also positioned near His178, but mutation of this residue had no discernible effect on toxicity (Fig. 4*B*). Asn149, Lys152, and Arg187 were tested for potential contributions to tRNA binding, but mutations at these positions also had no effect on growth inhibition (Fig. 4*B*). Lastly, we examined loop L2 residue Trp176, which is located at the junction with helix α3 near the putative catalytic triad of Asp155, His178, and Glu181 (Fig. 4*A*). Aromatic residues are conserved at this position in Ntox28 domains (Fig. S2*A*), suggesting that Trp176 may contribute to tRNA substrate recognition. The Trp176Ala expression plasmid was maintained stably in *cysK*$^+$ cells under repressive conditions, but cell growth was inhibited upon induction with arabinose (Fig. 4*B*). In vitro nuclease assays with purified toxins showed that the Asp155Ala, His178Ala, and Glu181Ala mutations each blocked activity (Fig. 4*C*). Additionally, we found that CdiA-CT^{EC536} anticodon nuclease activity requires divalent cations (Fig. S3*A*), suggesting that Asp155 and Glu181 may contribute to catalysis by coordinating Mg^{2+}. The Thr185Ile mutation had a minor effect, but the activity of the Trp176Ala variant was significantly attenuated (Fig. 4*C*). To exclude the possibility that the mutations

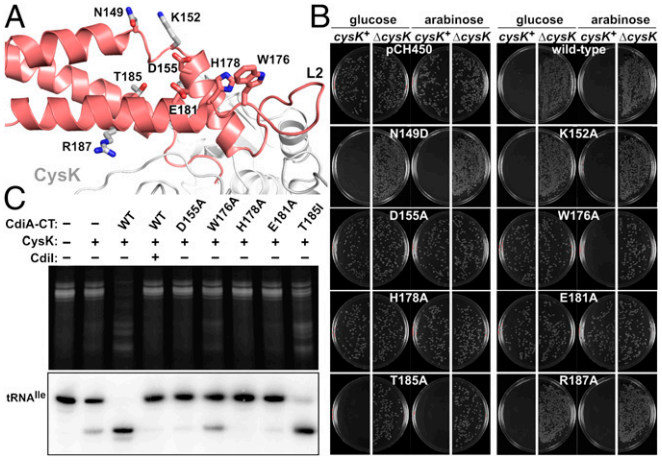

Fig. 4. Identification of nuclease active-site residues. (*A*) Mutated residues of CdiA-CT^{EC536}. (*B*) Growth inhibition activity of CdiA-CT^{EC536} variants. Arabinose-inducible expression plasmids were introduced into *E. coli cysK*$^+$ and Δ*cysK* cells, and transformants were selected on media supplemented with glucose or arabinose. Plasmid pCH450 is the empty vector. (*C*) In vitro nuclease activity of CdiA-CT^{EC536} variants. Purified CdiA-CT^{EC536} proteins were incubated with total cellular RNA in the presence of CysK and CdiI^{EC536} where indicated. Reactions were run on denaturing polyacrylamide gels and visualized by ethidium bromide staining (*Top*) and Northern blot hybridization (*Bottom*).

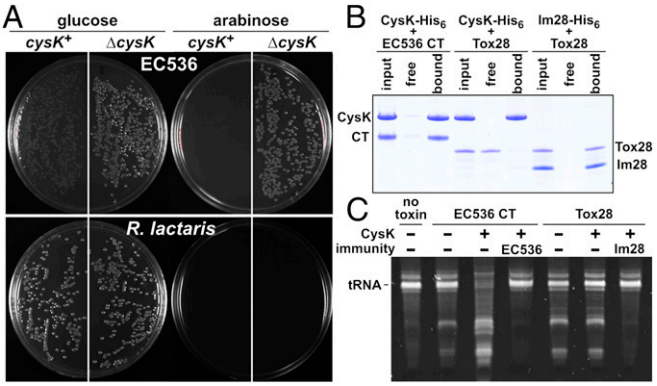

Fig. 5. *R. lactaris* Tox28 is a CysK-independent tRNase. (*A*) CdiA-CT/CdiI^{EC536}-DAS and Tox/Imm^{Rlac}-DAS expression constructs were introduced into *E. coli cysK*$^+$ and Δ*cysK* cells, and transformants were selected on media supplemented with glucose or arabinose. (*B*) Protein binding assays. The indicated proteins were mixed and subjected to Ni^{2+}-affinity chromatography. The free lanes represent proteins that failed to bind the affinity matrix, and the bound lanes show proteins eluted with imidazole. (*C*) In vitro nuclease assays. Purified CdiA-CT^{EC536} or Tox28^{Rlac} was incubated with total cellular RNA. Reactions were supplemented with purified CysK, CdiI^{EC536}, or Imm^{Rlac} where indicated.

interfere with CysK binding, we confirmed that each CdiA-CT^{EC536} variant interacts with CysK-His$_6$ using Ni^{2+}-affinity copurification (Fig. S3*B*). Together, these results suggest that Asp155, His178, and Glu181 form a catalytic triad required for tRNase activity.

Several CdiA proteins carry Ntox28 domains, and these toxins are also found at the C terminus of Tyr-Asp-repeat and WXG100 proteins from Gram-positive bacteria (4). Gram-positive Ntox28 domains have insertions in loop L3 and lack C-terminal G(Y/H)GI sequences (Fig. S2*A*), suggesting that they do not interact with CysK. We tested this prediction using the Ntox28/immunity protein pair encoded by the RUMLAC_00243/00244 loci of *R. lactaris* ATCC 29176. We first confirmed that Tox28^{Rlac} inhibits cell growth using controlled proteolysis to degrade ssrA(DAS)-tagged Imm^{Rlac} immunity protein, thereby liberating the toxin domain inside *E. coli* cells. Tox28^{Rlac} inhibited the growth of both *cysK*$^+$ and Δ*cysK* cells whereas expression of CdiA-CT^{EC536} using the same approach had no inhibitory effect on Δ*cysK* cells (Fig. 5*A*). We also found that CysK does not bind to Tox28^{Rlac} with high affinity although the toxin forms a stable complex with the Imm^{Rlac} immunity protein (Fig. 5*B*). In vitro nuclease assays revealed that purified Tox28^{Rlac} cleaves tRNA, but, in contrast to CdiA-CT^{EC536}, the addition of CysK failed to stimulate nuclease activity (Fig. 5*C*). Together, these results demonstrate that Tox28^{Rlac} shares tRNase activity with CdiA-CT^{EC536} but does not require activation by CysK or other proteins.

The autonomy of the Tox28^{Rlac} domain raises the question of why CdiA-CT^{EC536} requires activation. Because the CdiA-CT^{EC536} nuclease domain is small and lacks an extensive hydrophobic core, we explored the possibility that CysK stabilizes the toxin fold. We first monitored the stability of each toxin to thermal denaturation using circular dichroism (CD) spectroscopy. These analyses revealed that the melting temperature (T_m) for Tox28^{Rlac} is ∼10 °C higher than that of the CdiA-CT^{EC536} toxin (Table S6 and Fig. S4*A*). We then examined the thermostability of the CysK/CdiA-CT^{EC536} complex using both CD spectroscopy and differential scanning fluorimetry (DSF). Both experimental approaches showed that the CysK/CdiA-CT^{EC536} complex has a T_m of ∼66 °C, which is very similar to the value obtained for Tox28^{Rlac} (Table S6 and Fig. S4*A*). The T_m for isolated CysK was ∼58 °C (Table S6), showing that the complex is more stable than the individual components. We also found that the CdiI^{EC536} and Imm^{Rlac} immunity proteins

BIOCHEMISTRY

have a significant stabilizing effect, effectively increasing the T_m for each toxin (Table S6 and Fig. S4*B*). These data indicate that CdiA-CT^{EC536} is intrinsically less stable than Tox28^{Rlac} but exhibits comparable thermostability when bound to CysK.

Finally, we tested whether CysK promotes the binding of tRNA substrates to CdiA-CT^{EC536}. We expressed His_6 epitope-tagged CdiA-CT(H178A)^{EC536} and/or CysK in *E. coli* and then treated the cell lysates with formaldehyde to cross-link tRNA to the proteins. Analysis of complexes isolated from these reactions revealed that tRNA was preferentially cross-linked when both CysK and CdiA-CT^{EC536} were present in the lysates (Fig. 6*A*). This interaction appears to reflect physiologically relevant substrate binding because coexpression of CdiI^{EC536} reduced tRNA cross-linking to the CysK/CdiA-CT^{EC536} complex (Fig. 6*B*). This latter result suggests that immunity protein blocks nuclease activity by occluding the tRNA-binding site. Because Tox28^{Rlac} is an autonomous tRNase, we predicted that it should exhibit intrinsic tRNA-binding activity. We generated a His_6-tagged version of Tox28^{Rlac} that contains the His114Ala mutation to ablate nuclease activity and tested whether it binds substrate. Substantial amounts of tRNA copurified with the inactive Tox28^{Rlac} domain, even without formaldehyde cross-linking (Fig. 6*C*). The interaction between tRNA and Tox28^{Rlac} was effectively blocked by cognate Imm^{Rlac} immunity protein (Fig. 6*C*), again suggesting that the immunity protein binds over the nuclease active site. Together, these results indicate that CysK stabilizes CdiA-CT^{EC536}, rendering the nuclease domain competent to bind substrate. By contrast, the Tox28^{Rlac} domain is intrinsically stable and binds tRNA without assistance from CysK.

Discussion

These results provide several insights into CdiA-CT^{EC536} toxin activation. As predicted from prior work (8), the crystal structures show that the toxin inserts its C-terminal GYGI tail into the CysK active site and anchors the complex. The toxin's C-terminal carboxylate forms important H-bond contacts with conserved CysK active-site residues in the substrate-binding loop, and these same interactions are observed in the structures of CysE peptides bound to CysK from *Haemophilus influenzae* and *Arabidopsis thaliana* (21, 22). The C-terminal Ile residues of CdiA-CT^{EC536} and CysE exploit the same hydrophobic and H-bond contacts as *O*-acetylserine to bind the CysK active site (19). Although C-terminal Ile residues are critical for binding, substitutions are tolerated at other positions within the peptide tail. Salsi et al. have shown that CysK binds CysE peptides altered at the penultimate and antepenultimate positions (13). This plasticity accommodates the natural variation in CysE tail sequences and accounts for the ability of *E. coli* CysK to bind both GDGI and GYGI motifs with high affinity. Structures are not available for the full cysteine synthase complex; thus, it is unclear whether CdiA-CT^{EC536} mimics other features of CysE. However, we note that the CysE structure differs markedly from CdiA-CT^{EC536}. The CysE C-terminal domain forms a β-helix that terminates in a flexible tail (25). Further, the β-helical domain mediates trimerization, and two CysE trimers interact to form a larger homohexameric complex (25). If the β-helical domains of CysE interact with CysK, then the contacts are likely to be distinct from those observed with the CdiA-CT^{EC536} α-helical bundle. The same uncertainties apply to other "moonlighting" partners of CysK for which no structural information is available (15). It is intriguing that CysK has been repeatedly recruited as a binding partner by disparate proteins. Perhaps this phenomenon reflects the antiquity and immutability of cysteine synthase complexes, which remain remarkably similar in extant bacteria and plants. From the perspective of CDI, the ubiquity and conserved active-site architecture of CysK ensure that toxins can be activated in a broad range of bacteria.

The structure of the CdiA-CT^{EC536} nuclease domain is unique, and its catalytic mechanism seems to be distinct from other anticodon nucleases. Colicins E5 and D are the only other anticodon nucleases for which structures are available (26). The nuclease domains of colicins E5 and D share an α/β fold that characterizes the Barnase-EndoU-ColicinE5/D-RelE (BECR) family of RNases (4). Like barnase, colicins E5 and D are metal-independent nucleases that abstract a proton from the 2′-hydroxyl to initiate an intramolecular attack on the scissile phosphodiester bond (26). By contrast, CdiA-CT^{EC536} has divalent cation-dependent nuclease activity, which is usually associated with a hydrolytic mechanism. Mutational analyses support a role for CdiA-CT^{EC536} residues Asp155, Glu181, and His178 in catalysis. Asp155 and Glu181 are candidates to coordinate Mg^{2+}, which could either activate water for hydrolysis or stabilize hydroxide ions generated by His178 acting as a general base (27). Another difference between colicins E5/D and CdiA-CT^{EC536} is the lack of a defined substrate-binding pocket in the latter nuclease. Several observations suggest that flexible loop L2 participates in tRNA binding. L2 is conserved among Ntox28 family members and always contains hydrophobic residues adjacent to His178. Our results show that Trp176 is important, but not strictly required, for CdiA-CT^{EC536} activity. We hypothesize that Trp176 stacks onto nucleobases within the tRNA anticodon loop. This mode of recognition is common among aminoacyl-tRNA synthetases, which bind cognate tRNAs using conserved hydrophobic/aromatic residues that stack onto the first and second nucleotides of the anticodon (28).

Finally, we propose that CysK promotes CdiA-CT^{EC536} nuclease activity by stabilizing the toxin's fold. The CdiA-CT^{EC536} helical bundle is relatively small and lacks an extensive hydrophobic core. Consequently, CdiA-CT^{EC536} has relatively low thermostability, raising the possibility that thermal fluctuations disrupt the active site by splaying the helices. CysK anchors toxin helices α2 and α3, thereby approximating Asp155 and Glu181 to coordinate Mg^{2+}. The CysK scaffold also anchors the ends of loop L2, which we propose is important for substrate binding. In support of this model, we find that tRNA interacts with the CysK/CdiA-CT^{EC536} complex, but not with the individual components. CdiI^{EC536} blocks the interaction with substrate, strongly suggesting that the immunity protein occludes the nuclease active site. The extensive contact between loop L2 and CdiI^{EC536}, together with the sequestration of Trp176 within the immunity protein, is consistent with this model. Although CysK is critical for CdiA-CT^{EC536} nuclease activity, related toxins from Gram-positive bacteria probably do not require extrinsic activation because purified Tox28 domain from *R. lactaris* has tRNase activity in vitro. Ntox28 domains are typically found at the C terminus of proteins that mediate interbacterial competition (4, 29–31). For example, the *R. lactaris* Tox28^{Rlac} domain is part of a larger

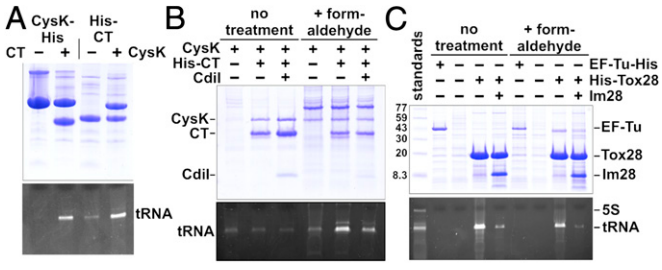

Fig. 6. tRNA binding to Ntox28 nuclease domains. (*A*) Cross-linking of tRNA to CysK/CdiA-CT^{EC536} complexes. *E. coli* cell lysates containing CysK and/or CdiA-CT (H178A)^{EC536} were treated with formaldehyde, and cross-linked nucleoprotein complexes were purified by Ni^{2+}-affinity chromatography. Purified samples were analyzed by SDS/PAGE (*Top*) and 50% urea PAGE (*Bottom*) to visualize proteins and nucleic acid, respectively. (*B*) CdiI^{EC536} blocks tRNA cross-linking to CysK/CdiA-CT^{EC536}. *E. coli* cell lysates containing CysK-His_6, CysK-His_6/CdiA-CT(H178A)^{EC536}, and CysK-His_6/CdiA-CT(H178A)/CdiI^{EC536} were treated with formaldehyde where indicated, followed by Ni^{2+}-affinity chromatography, and gel analysis as described in *A*. (*C*) Tox28^{Rlac} interacts stably with tRNA substrate. Cell lysates containing His_6-Tox28(H114A)^{Rlac} and Imm^{Rlac} were treated as described above. To ascertain cross-linking specificity, EF-Tu-His_6 was also purified and analyzed for tRNA binding.

rearrangement hotspot (Rhs) repeat protein. Rhs and related YD-repeat proteins deliver toxic nuclease domains into both Gram-negative and Gram-positive bacteria (32, 33). Further, the Ntox28 homolog from *Geobacillus* sp. strain Y412MC10 (GYMC10_1092) is linked to an N-terminal ESAT-6–like domain, which is predicted to guide export through type VII secretion systems (4, 29). Given that all Ntox28 domains function in intercellular competition, perhaps the mechanism of toxin delivery into Gram-negative bacteria accounts for the relative instability of CdiA-CT^{EC536}. We recently discovered that CDI toxins hijack a variety of inner-membrane proteins to enter the target-cell cytoplasm (9). If CdiA-CT domains must unfold during this translocation step, then there may be a selective pressure for toxins with low global stability.

Methods

Plasmid constructions (Table S7), site-directed mutagenesis, and protein purification procedures are described in *SI Methods* (8). Protein crystallization was previously described (6). Briefly, crystals were grown by the hanging-drop, vapor-diffusion method at room temperature against a reservoir containing 0.2 M $NaSO_4$, 0.1 M Bis-Tris propane (pH 7.9), and 20% (wt/vol) PEG 3350, for the binary complex, and 0.1 M sodium cacodylate (pH 7.1), 0.2 M ammonium sulfate, and 17% (wt/vol) PEG-8000, for the ternary complex. Structural models were determined as described (6). Protein binding affinities were calculated using biolayer interferometry, and thermal stabilities were determined by DSF and CD spectroscopy as outlined in *SI Methods*. Nuclease activity assays were performed as described (8) with modifications outlined in *SI Methods*. Nucleoprotein cross-linking was performed as described in *SI Methods*.

ACKNOWLEDGMENTS. We thank the Stanford Synchrotron Radiation Lightsource (SSRL) and the Advanced Light Source (ALS) at Berkeley National Laboratory for invaluable help in data collection; and Xin Liu for technical support. This work was supported by National Institutes of Health Grant GM102318 (to C.W.G., C.S.H., and D.A.L.). P.M.J. was supported in part by University of California, Irvine Bridge Funding, and C.M.B. was supported in part by a University of California, Santa Barbara Dean's Fellowship and the Chang Fellowship.

1. Willett JL, Ruhe ZC, Goulding CW, Low DA, Hayes CS (2015) Contact-dependent growth inhibition (CDI) and CdiB/CdiA two-partner secretion proteins. *J Mol Biol* 427(23):3754–3765.
2. Ruhe ZC, Wallace AB, Low DA, Hayes CS (2013) Receptor polymorphism restricts contact-dependent growth inhibition to members of the same species. *MBio* 4(4): e00480-13.
3. Aoki SK, et al. (2010) A widespread family of polymorphic contact-dependent toxin delivery systems in bacteria. *Nature* 468(7322):439–442.
4. Zhang D, de Souza RF, Anantharaman V, Iyer LM, Aravind L (2012) Polymorphic toxin systems: Comprehensive characterization of trafficking modes, processing, mechanisms of action, immunity and ecology using comparative genomics. *Biol Direct* 7:18.
5. Beck CM, et al. (2014) CdiA from *Enterobacter cloacae* delivers a toxic ribosomal RNase into target bacteria. *Structure* 22(5):707–718.
6. Morse RP, et al. (2012) Structural basis of toxicity and immunity in contact-dependent growth inhibition (CDI) systems. *Proc Natl Acad Sci USA* 109(52):21480–21485.
7. Nikolakakis K, et al. (2012) The toxin/immunity network of *Burkholderia pseudomallei* contact-dependent growth inhibition (CDI) systems. *Mol Microbiol* 84(3):516–529.
8. Diner EJ, Beck CM, Webb JS, Low DA, Hayes CS (2012) Identification of a target cell permissive factor required for contact-dependent growth inhibition (CDI). *Genes Dev* 26(5):515–525.
9. Willett JL, Gucinski GC, Fatherree JP, Low DA, Hayes CS (2015) Contact-dependent growth inhibition toxins exploit multiple independent cell-entry pathways. *Proc Natl Acad Sci USA* 112(36):11341–11346.
10. Kredich NM, Becker MA, Tomkins GM (1969) Purification and characterization of cysteine synthetase, a bifunctional protein complex, from *Salmonella typhimurium*. *J Biol Chem* 244(9):2428–2439.
11. Zhao C, et al. (2006) On the interaction site of serine acetyltransferase in the cysteine synthase complex from *Escherichia coli*. *Biochem Biophys Res Commun* 341(4):911–916.
12. Chattopadhyay A, et al. (2007) Structure, mechanism, and conformational dynamics of O-acetylserine sulfhydrylase from Salmonella typhimurium: Comparison of A and B isozymes. *Biochemistry* 46(28):8315–8330.
13. Salsi E, et al. (2010) Design of O-acetylserine sulfhydrylase inhibitors by mimicking nature. *J Med Chem* 53(1):345–356.
14. Campanini B, et al. (2005) Interaction of serine acetyltransferase with O-acetylserine sulfhydrylase active site: Evidence from fluorescence spectroscopy. *Protein Sci* 14(8):2115–2124.
15. Campanini B, et al. (2015) Moonlighting O-acetylserine sulfhydrylase: New functions for an old protein. *Biochim Biophys Acta* 1854(9):1184–1193.
16. Tanous C, et al. (2008) The CymR regulator in complex with the enzyme CysK controls cysteine metabolism in *Bacillus subtilis*. *J Biol Chem* 283(51):35551–35560.
17. Ma DK, Vozdek R, Bhatla N, Horvitz HR (2012) CYSL-1 interacts with the O2-sensing hydroxylase EGL-9 to promote H2S-modulated hypoxia-induced behavioral plasticity in *C. elegans*. *Neuron* 73(5):925–940.
18. Burkhard P, et al. (1998) Three-dimensional structure of O-acetylserine sulfhydrylase from *Salmonella typhimurium*. *J Mol Biol* 283(1):121–133.
19. Burkhard P, Tai CH, Ristroph CM, Cook PF, Jansonius JN (1999) Ligand binding induces a large conformational change in O-acetylserine sulfhydrylase from *Salmonella typhimurium*. *J Mol Biol* 291(4):941–953.
20. Morse RP, et al. (2015) Diversification of β-augmentation interactions between CDI toxin/immunity proteins. *J Mol Biol* 427(23):3766–3784.
21. Huang B, Vetting MW, Roderick SL (2005) The active site of O-acetylserine sulfhydrylase is the anchor point for bienzyme complex formation with serine acetyltransferase. *J Bacteriol* 187(9):3201–3205.
22. Francois JA, Kumaran S, Jez JM (2006) Structural basis for interaction of O-acetylserine sulfhydrylase and serine acetyltransferase in the *Arabidopsis* cysteine synthase complex. *Plant Cell* 18(12):3647–3655.
23. Claus MT, Zocher GE, Maier TH, Schulz GE (2005) Structure of the O-acetylserine sulfhydrylase isoenzyme CysM from Escherichia coli. *Biochemistry* 44(24):8620–8626.
24. Holm L, Rosenstrom P (2010) Dali server: Conservation mapping in 3D. *Nucleic Acids Res* 38(Web Server issue):W545–W549.
25. Hindson VJ, Moody PC, Rowe AJ, Shaw WV (2000) Serine acetyltransferase from *Escherichia coli* is a dimer of trimers. *J Biol Chem* 275(1):461–466.
26. Papadakos G, Wojdyla JA, Kleanthous C (2012) Nuclease colicins and their immunity proteins. *Q Rev Biophys* 45(1):57–103.
27. Dupureur CM (2008) Roles of metal ions in nucleases. *Curr Opin Chem Biol* 12(2): 250–255.
28. Beuning PJ, Musier-Forsyth K (1999) Transfer RNA recognition by aminoacyl-tRNA synthetases. *Biopolymers* 52(1):1–28.
29. Zhang D, Iyer LM, Aravind L (2011) A novel immunity system for bacterial nucleic acid degrading toxins and its recruitment in various eukaryotic and DNA viral systems. *Nucleic Acids Res* 39(11):4532–4552.
30. Poole SJ, et al. (2011) Identification of functional toxin/immunity genes linked to contact-dependent growth inhibition (CDI) and rearrangement hotspot (Rhs) systems. *PLoS Genet* 7(8):e1002217.
31. Holberger LE, Garza-Sánchez F, Lamoureux J, Low DA, Hayes CS (2012) A novel family of toxin/antitoxin proteins in *Bacillus* species. *FEBS Lett* 586(2):132–136.
32. Koskiniemi S, et al. (2013) Rhs proteins from diverse bacteria mediate intercellular competition. *Proc Natl Acad Sci USA* 110(17):7032–7037.
33. Whitney JC, et al. (2014) Genetically distinct pathways guide effector export through the type VI secretion system. *Mol Microbiol* 92(3):529–542.
34. Aiyar A, Leis J (1993) Modification of the megaprimer method of PCR mutagenesis: Improved amplification of the final product. *Biotechniques* 14(3):366–369.
35. Otwinowski Z, Minor W (1997) Processing of X-ray diffraction data collected in oscillation mode. *Methods Enzymol* 276:307–326.
36. Adams PD, et al. (2010) PHENIX: A comprehensive Python-based system for macromolecular structure solution. *Acta Crystallogr D Biol Crystallogr* 66(Pt 2):213–221.
37. Emsley P, Lohkamp B, Scott WG, Cowtan K (2010) Features and development of Coot. *Acta Crystallogr D Biol Crystallogr* 66(Pt 4):486–501.
38. Garza-Sánchez F, Janssen BD, Hayes CS (2006) Prolyl-tRNA(Pro) in the A-site of SecM-arrested ribosomes inhibits the recruitment of transfer-messenger RNA. *J Biol Chem* 281(45):34258–34268.
39. Beckwith JR, Signer ER (1966) Transposition of the lac region of Escherichia coli. I. Inversion of the lac operon and transduction of lac by phi80. *J Mol Biol* 19(2):254–265.